SPECIAL ISSUE - ORIGINAL ARTICLE

Patient-specific flow analysis of brain aneurysms at a single location: comparison of hemodynamic characteristics in small aneurysms

Aichi Chien · Satoshi Tateshima · Marcelo Castro · James Sayre · Juan Cebral · Fernando Viñuela

Abstract The purpose of this study is to examine and compare the hemodynamic characteristics of small aneurysms at the same anatomical location. Six internal carotid artery-ophthalmic artery aneurysms smaller than 10 mm were selected. Image-based computational fluid dynamics (CFD) techniques were used to simulate aneurysm hemodynamics. Flow velocity and wall shear stress (WSS) were also quantitatively compared, both in absolute value and relative value using the parent artery as a baseline. We found that flow properties were similar in ruptured and unruptured small aneurysms. However, the WSS was lower at the aneurysm site in unruptured aneurysms and higher in ruptured aneurysms ($P < 0.05$). Hemodynamic analyses at a single location with similar size enabled us to directly compare the hemodynamics and clinical presentation of brain aneurysms. The results suggest that the WSS in an aneurysm sac can be an important hemodynamic parameter related to the mechanism of brain aneurysm growth and rupture.

Keywords Flow analysis · Hemodynamics · Brain aneurysm

A. Chien (✉) · S. Tateshima · F. Viñuela
Division of Interventional Neuroradiology, David Geffen School of Medicine, University of California, 10833 LeConte Ave., Box 951721, Los Angeles, CA 90095, USA
e-mail: achien@mednet.ucla.edu

M. Castro · J. Cebral
Department of Computational Sciences, George Mason University, Fairfax, VA 22030, USA

J. Sayre
Department of Biostatistics, School of Public Health, University of California, Los Angeles, CA 90095, USA

1 Introduction

Anatomical parameters help predict the natural history of brain aneurysms. For instance, it is known that the risk of rupture greatly increases as the aneurysm becomes larger [26, 30, 31]. The International Study on unruptured intracranial aneurysms (ISUIA) and many other clinical reports have also indicated the risk of aneurysm rupture varies with aneurysm location [26, 30, 31]. Recent reports have supported the concept that there is a difference in shape between ruptured and unruptured aneurysms [2, 13, 15, 28, 29]. Their results indicate that aneurysms which have a higher aspect ratio or have irregular shapes are more likely to rupture.

Intra-aneurysmal hemodynamics is believed to be another important factor related to the etiology and natural history of brain aneurysms [3, 4, 6, 7, 10, 17, 18, 21, 22]. Recent hemodynamic studies have used patient angiographic data to perform flow simulation, because vascular and aneurysm geometries have a significant influence upon the intra-aneurysmal flow pattern [4, 22]. A few studies using patient-specific data have demonstrated differences in the intra-aneurysmal hemodynamic patterns between ruptured and unruptured aneurysms [6, 17]. However, due to the limited number of available cases, such analyses have included aneurysms from various locations, different sizes, and a variety of aneurysm shapes. Variation between ruptured and unruptured aneurysms is thus combined with hemodynamic variation caused by other factors, making it difficult to specifically compare results between ruptured and unruptured aneurysms. Therefore, it remains unanswered whether there is a hemodynamic difference between ruptured and unruptured aneurysms when size is similar between them and they share the same anatomical location. In this study, we introduce a new approach to

analyze brain aneurysms by studying cases from a single location with the same approximate size. We qualitatively and quantitatively compare differences in flow properties and wall shear stress. Additionally, we present a method to reduce parameters influencing hemodynamic properties which can be useful to design a larger hemodynamic study for brain aneurysm disease.

2 Methods

2.1 Case selection

Internal carotid artery-ophthalmic artery (IC-Oph) aneurysms were selected, as they are the most common in our 3D rotational digital subtraction angiography database [12]. Patients who were enrolled from 2003 to 2007 with ruptured or unruptured IC-Oph aneurysms were screened, and a total of 22 IC-Oph aneurysms with 3D rotational angiograms were found. Images for unruptured aneurysms were taken during a patient's clinical evaluation. Images documenting ruptured aneurysms were taken within 24 h after the event of aneurysm rupture. To minimize the possible hemodynamic variation caused by the size and shape of aneurysm domes and to maximize the number of cases, we selected cases with the greatest diameter less than 10 mm, following the 1998 ISUIA small aneurysm definition [26]. Aneurysms with angiographic evidence of vasospasm in the parent artery were also excluded because vasospasm may alter the intra-aneurysmal hemodynamics significantly [20]. Thus, a total of six small IC-Oph aneurysms (four unruptured and two ruptured) were included in this study (Table 1).

2.2 Image acquisition

Three-dimensional rotational cerebral angiography was acquired using a Philips Integris unit (Philips Medical Systems, Best, The Netherlands) before aneurysm embolization. Data from these images was transferred to the Philips Integris workstation for 3D voxel generation and image restoration.

2.3 Computational fluid dynamics simulation

The 3D voxel data obtained by rotational angiography was then transferred to a Dell 490 workstation for the CFD simulation. Image-based CFD software developed by Cebral et al., was used for aneurysmal model reconstruction and flow simulation. For each aneurysm, the 3D computational model was constructed semi-automatically through segmentation, surface generation, and 3D grid generation, based on deformable models and the level set method. Details of this process are described in [4–7, 32]. To incorporate 3D geometry into the flow analysis, computational meshes were generated for each model with approximately 1,500,000 tetrahedral elements.

The pulsatile flow conditions measured from a normal subject's internal carotid arteries (ICA) using MR phase contrast measurements (General Electric 1.5T scanner, Waukesha, WI, USA) were imposed on the CFD model [6]. It was scaled according to the cross-sectional area of the inflow vessels for the models (Table 1) to maintain the WSS level and assumed to be constant among individuals [8, 16]. The traction-free boundary condition was applied for the outflow condition at the internal carotid arteries. At the ophthalmic arteries, the outflow was imposed according to a flow division based on the cross-sectional areas. Since previous work has shown that there is no significant difference in hemodynamic characteristics comparing Newtonian flow and non-Newtonian flow [7], in our simulation, the unsteady, incompressible Navier–Stokes equations were numerically solved under the Newtonian fluid assumption. A fully implicit finite element formulation which allows arbitrary time-step size was used in the computational method [7, 19].

Blood was modelled with a viscosity of 0.004 Pascal-second and a density of 1,000 kg/m³. Arteries have a complex elastic component and it is not uncommon to find regionally calcified aneurysm wall [25]. To include the elastic properties in the computation, knowledge about the material composition and the proper elastic formulation to describe the walls of each aneurysm are needed. Currently, information about elastic properties of specific walls and wall uniformity, the key components to

Table 1 Geometrical information about the aneurysms used in the hemodynamical simulation

	A	B	C	D	E	F
Aneurysm depth (mm)	3.1	6.2	6.9	5.4	6.6	6.1
Aneurysm neck (mm)	4.0	4.5	6.5	3.3	5.2	4.1
Aneurysm body (mm)	3.8	7.3	6.3	4.8	7.7	7.0
Maximum dimension (mm)	4.0	7.3	6.9	5.4	7.7	6.9
Aspect ratio (aneurysm depth/aneurysm neck)[a]	0.78	1.37	1.06	1.63	1.27	1.49
Inflow vessel cross- sectional area (mm²)	20.9	14.7	18.7	17.6	13.4	12.2
Ruptured (R) or unruptured (U)	R	R	U	U	U	U

[a] Calculation was based on Ujiie et al. [28]

determine tissue deformation, is not yet obtainable. Therefore, in this study, the rigid and no-slip boundary condition was prescribed at the vessel wall. Viscoelastic properties of the vessel wall were neglected [6, 17]. Although the assumption of a rigid boundary may not reflect the elastic nature of the blood vessel, it simplifies the computation and provides a consistent way to study the hemodynamic effect.

2.4 Results analysis

The CFD results were analyzed quantitatively and qualitatively. The qualitative categorization was performed following the classification proposed by Cebral et al. [6]. Flow properties such as 3D flow pattern, streamlines in the aneurysm sac, locations of flow impingement (impingement location), and impingement size were examined. Limiting streamlines (LS) to study complicated three-dimensional flow separation [11, 27] and WSS patterns to evaluate the hemodynamic stress caused by the blood flow [17, 23] were also analyzed for each aneurysm. The categorization for each aneurysm was performed by both A. C. and S. T independently. In the situation of disagreements in categorizations, re-examination was performed to reach a consensus. This was to ensure the flow properties were fully evaluated and the categorizations were appropriate.

Because there are still dimensional differences between aneurysms, the quantitative flow properties were sampled from six cut planes for each aneurysm model to compare values such as the blood flow velocity and wall shear stress (Fig. 1). The planes crossed the parent artery at the proximal end of the aneurysm dome (P1), center of the aneurysm dome (P2), and distal end of the aneurysm dome (P3); planes at the level of the aneurysm neck (A1), middle (A2), and top (A3). The location of each aneurysm neck was determined by two experienced interventional neuroradiologists (S. T. and F. V.) together to ensure the location was accurate and consistent.

Flow velocity and WSS for the peak pulsatile flow was extracted from computational points in each cut plane. Raw data was compared to find differences in absolute values between ruptured and unruptured aneurysms. Because aneurysms result from arterial malformation, analyses to compare the flow properties between each aneurysm sac and parent artery were also performed [23, 26]. We first calculated the average flow velocity in the aneurysm's parent artery. Then, this value was used as a baseline for the relative flow velocity across a specific plane (Eq. 1). Likewise, for a particular plane, the relative WSS was defined as the average wall shear stress at that plane divided by the average WSS at the parent artery planes (Eq. 2).
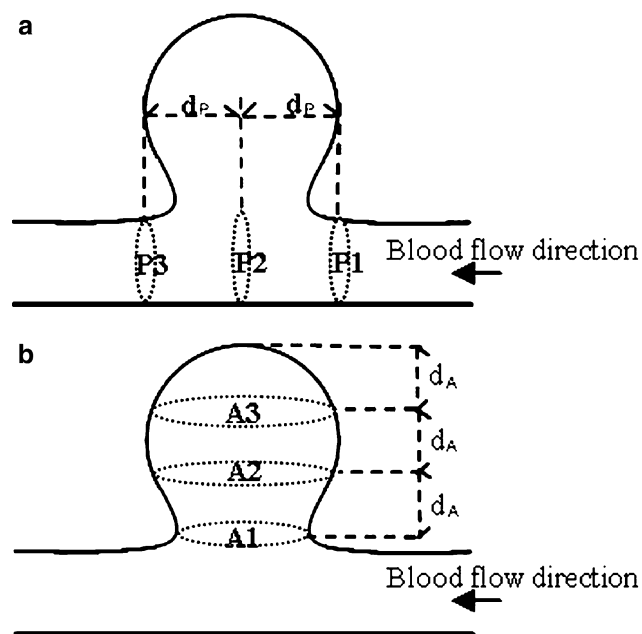

Fig. 1 Schematic representation of planes for the hemodynamic quantitative analyses. **a** The parent artery has three cross-sectional planes defined perpendicular to the natural axis of the artery, corresponding to the proximal end of the aneurysm sac (P1), center of the aneurysm sac (P2), and distal end of the aneurysm sac (P3). Distance (d_P) between P1 and P2 is the same as the distance between P2 and P3. **b** Three planes in the aneurysm sac were defined by dividing the height of the aneurysm by the same distance (d_A) from the aneurysm neck to the aneurysm apex. Three planes were defined at the aneurysm neck (A1), middle (A2), and top (A3)

$$\frac{\text{(average flow velocity at a specific plane)}}{\text{(average flow velocity at parent artery planes)}}$$
$$= \text{relative flow velocity} \qquad (1)$$

$$\frac{\text{average WSS at a specific plane}}{\text{average WSS at parent artery planes}} = \text{relative WSS} \qquad (2)$$

2.5 Statistical methods

Statistical methods were used to analyze how hemodynamic parameters associate with aneurysm rupture. Quantitative results are expressed as mean value and standard deviation. Descriptive statistics and Mann–Whitney test were performed to compare groups using SPSS 13.0 statistical software. Statistical significance was indicated at the 5% level.

3 Results

3.1 Blood flow patterns in the aneurysms

Flow patterns at the peak of pulsatile flow were analyzed. Figure 2a shows the flow velocity streamlines for each aneurysm. Blood flow direction, from proximal to distal of

Fig. 2 Blood flow patterns in ruptured aneurysms (A, B) and unruptured aneurysms (C–F). *Red arrows* indicate the blood flow directions. *Blue arrows* show the viewing directions to see the flow pattern (*yellow arrows*). Among the six aneurysms, only case B showed a blood flow pattern with multiple vortices. The rest of the aneurysms had a single vortex. Case A, B, D, and F had blood flow impingement at the neck of the aneurysm. Case C and E had blood flow impingement at the body and dome of the aneurysm, respectively
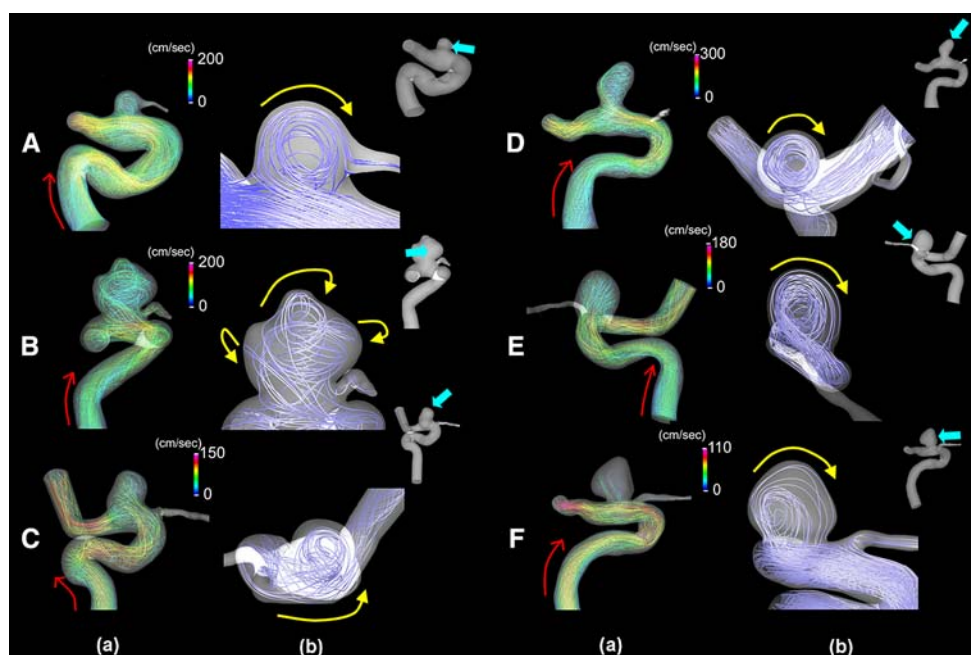
Table 2 Blood flow characteristics in internal carotid artery-ophthalmic artery aneurysms

	No.	Flow direction		Impingement location			Impingement size		Low WSS location	
		A single vortex	Multiple vortices	Neck	Body	Apex	Small	Large	Aneurysm	More evenly distributed
Ruptured	2	1	1	2			1	1		2
Unruptured	4	4		2	1	1	2	2	4	

the ICA is indicated by red arrows. At the site of an aneurysm, part of the flow enters the aneurysm and recirculates, forming vortices. Figure 2b shows the best angle to view the flow pattern for each aneurysm. Blue arrows show the viewing direction with respect to the aneurysm. In aneurysms A and C–F blood inflow into the aneurysm formed a single vortex (yellow arrows). Case B had the blood inflow split into three vortices in the aneurysm dome. The impingement locations were also analyzed [6]. Aneurysms A, B, D and F had blood inflow impinging at the neck. Aneurysms C and D had impingement at the body and the apex of the aneurysm, respectively. The impingement size in aneurysm B, D and F was small, less than half the size of the reference dimension (ie, neck or dome diameters) [6]. The results are summarized in Table 2. After comparing these properties, distinguishable differences were not found between ruptured and unruptured small aneurysms.

3.2 Limiting streamlines and wall shear stress distribution

Limiting streamlines (LS) are interpreted as trajectories arising from the vector-valued WSS on the surface. Three-dimensional flow separation has been defined as limiting streamlines converging onto one particular limiting streamline that originates from a saddle point [27]. Figure 3b and c show the side and top views of LS for each aneurysm indicating focus (LS spiral around the focus) and saddle points (two particular LS pass through the point, but all other LS miss it). Detailed information about LS can be found in [11, 27]. As shown in Fig. 3b and c, aneurysm A has a focus at the aneurysm dome, one saddle point at the junction of the aneurysm and ophthalmic artery, and another saddle point near the neck of the aneurysm (not visible in those views). In aneurysm B, a focus at the bulb area, two saddle points at the aneurysm body (one is not visible in those views), and one additional saddle point at the aneurysm neck were found. In aneurysm C, a saddle point at the neck of the aneurysm and a focus (top view) can be clearly seen. In aneurysm D, a saddle point near the aneurysm neck and a focus at the apex of the aneurysm were observed. In aneurysm E, a saddle point at the neck of the aneurysm and a focus at the body of the aneurysm were found. In aneurysm F, a focus and a saddle point were seen near the neck of the aneurysm.

We found that in the unruptured aneurysms, the magnitude of WSS was lower at the aneurysm site in comparison with the WSS at the parent artery (Fig. 3a, C–F). The highest WSS area was located at the ophthalmic

Fig. 3 a Wall shear stress (*WSS*) distributions, **b** side view of limiting streamlines (*LS*), **c** top view of LS in ruptured aneurysms (A and B) and unruptured aneurysms (C–F). In the ruptured aneurysms, the WSS at the aneurysm sacs was closer to the WSS at the parent artery. In the unruptured aneurysm, a lower WSS at the aneurysm sacs was observed (*dark blue*) when compared with the WSS at the parent artery (*green*). Locations of foci where LS spiral around a point are indicated. Saddle points (*SP*) where two particular LS pass through a point, but all other LS miss are also labelled
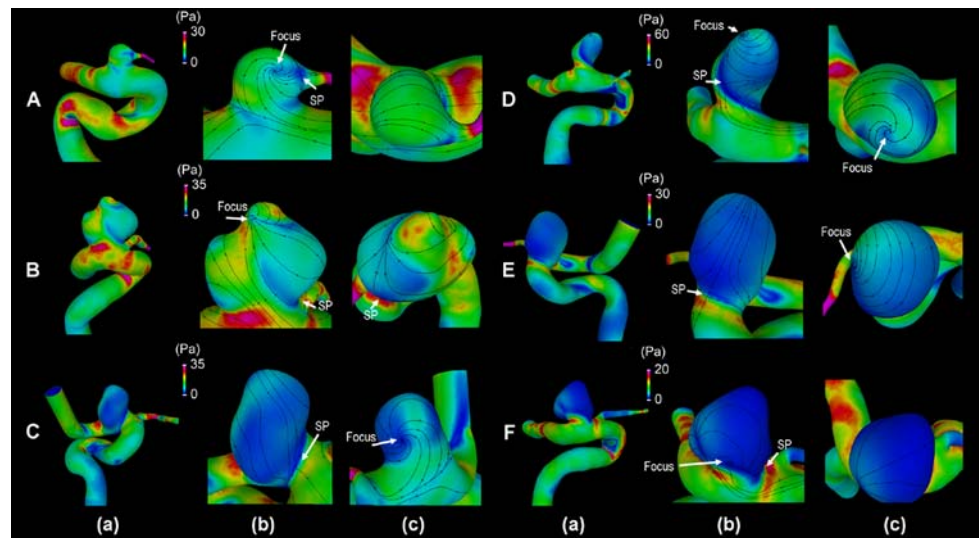
artery, followed by the distal and proximal regions of the IC artery (parent artery). In the ruptured aneurysms, the WSS at the aneurysm site appeared to be closer to the distribution at the parent artery (Fig. 3a, A and B). The highest WSS area was also located at the ophthalmic artery, followed by proximal regions of the IC artery. Higher regional WSS was also found in the ruptured aneurysm sacs, than in the unruptured cases (the aneurysm neck in case A and the aneurysm bulb in case B).

3.3 Quantitative analysis

The CFD results during peak pulsatile flow were analyzed for each aneurysm. The mean values of the flow velocity in the ruptured and unruptured aneurysms were 46.1 ± 16.6 and 40.9 ± 21.4 cm/s, respectively ($P = 0.856$). The mean WSS in the ruptured and unruptured aneurysms was 12.0 ± 6.4 and 10.2 ± 7.8 Pa, respectively ($P = 0.199$).

We also compared values of relative flow velocity and relative WSS within each aneurysm. The relative flow velocities at different planes of the parent arteries and aneurysm sacs are shown in Fig. 4a and b, respectively. In the ruptured aneurysms, the relative flow velocity was $100 \pm 16.9\%$ in the parent artery and $70.5 \pm 12.9\%$ in the aneurysm sac. In the unruptured aneurysms, the relative flow velocity was $100 \pm 13.9\%$ in the parent artery and $62.1 \pm 30.1\%$ in the aneurysm sac. Note that case F had very low flow velocity in the aneurysm sac, consistent with the limited flow pattern inside the aneurysm sac shown in Fig. 2. Comparing the ruptured and unruptured aneurysms, there were no statistical differences found in relative velocity values either in the parent artery ($P = 1.000$) or in the aneurysms sac ($P = 0.682$).

The relative WSS at different planes of the parent arteries and aneurysm sacs is shown in Fig. 5a and b,

respectively. In the ruptured aneurysms, the relative WSS was $100 \pm 26.09\%$ in the parent artery and $72.3 \pm 5.5\%$ at planes in the aneurysm sac. In the unruptured aneurysms, we found that the relative WSS was $100 \pm 22.5\%$ in the parent artery and $41.2 \pm 21.2\%$ in the aneurysm sacs, which includes one unruptured aneurysm with 63.6% relative WSS (case D). The relative WSS in the sac of ruptured aneurysms was significantly higher than the sac of unruptured aneurysms ($P = 0.003$). The relative WSS in parent arteries was not statically different between ruptured and unruptured cases ($P = 0.851$).

4 Discussion

Because of the diversity of brain aneurysms and a lack of methods to study aneurysm natural history, understanding of the mechanism underlying this disease is very limited [6, 21, 25]. We addressed this by analyzing aneurysms with similar size and shape in the same anatomical location, making hemodynamic properties more directly comparable between ruptured and unruptured groups. We were able to quantify variation of hemodynamic properties between cases.

Flow properties and LS were highly influenced by the aneurysm geometry. A small aneurysm with a smooth contour was more likely to have a single vortex, and multiple vortices might form from a small change in the aneurysm dome (Fig. 2, aneurysm B). LS showed that flow separation occurred near the neck of the aneurysms for all of the cases. For the ruptured aneurysms, in the one with the ophthalmic artery connecting to the dome, aneurysm A, additional flow separation at the connection was observed. In the other ruptured aneurysm, aneurysm B, we also found additional flow separation at the body of the aneurysm.
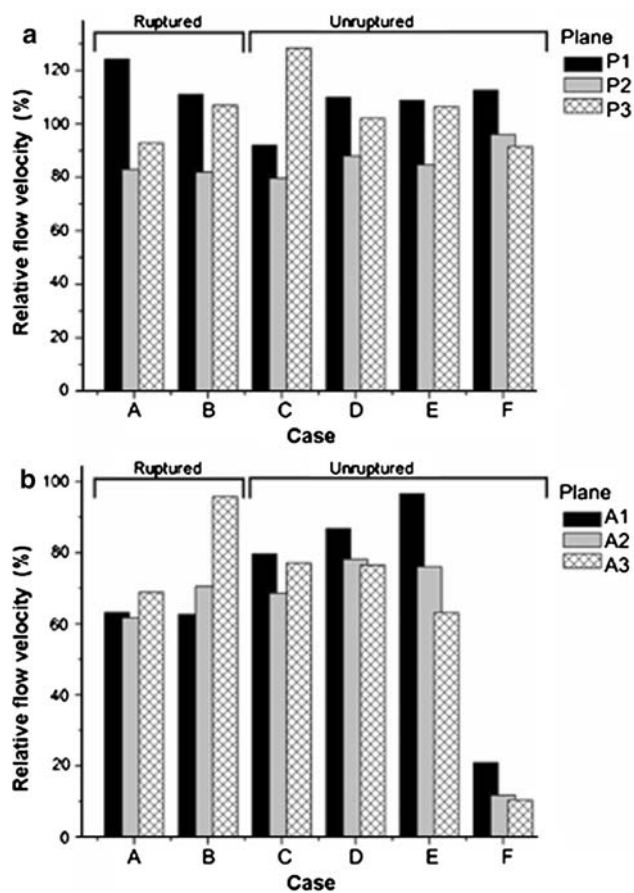
Fig. 4 Relative flow velocity in six aneurysms. A–F correspond to the cases shown in Fig. 2. Case A and B are ruptured aneurysms. Case C–F are unruptured aneurysms. P1, P2, P3, A1, A2, A3 are the planes indicated in Fig. 1. **a** The relative flow velocity in the parent arteries and showed no distinguishable difference between ruptured and unruptured aneurysms. **b** The relative flow velocity in aneurysm sacs. Variations between individuals can be observed, but there is no clear difference between ruptured and unruptured aneurysms. Note that case F had very low flow velocity in the aneurysm sac. This is consistent with the limited flow pattern within the aneurysm sac shown in Fig. 2
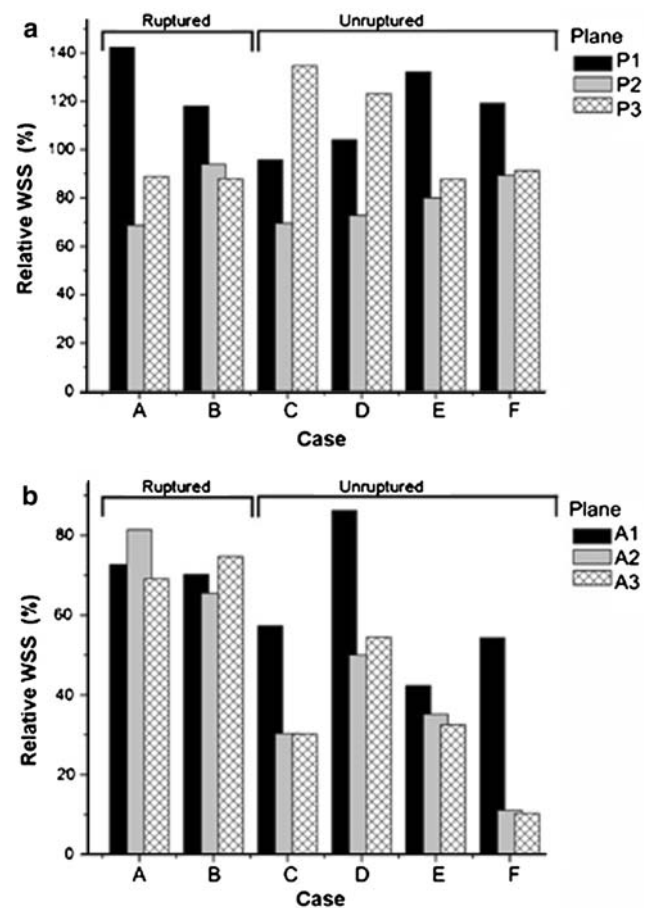

Fig. 5 Relative wall shear stress (WSS) in different locations for six aneurysms, following the same arrangement as Fig. 4. **a** The relative WSS along the parent arteries which showed no distinguishable difference between ruptured and unruptured aneurysms. **b** The relative WSS at the aneurysm sac. The relative WSS at the aneurysm sac is higher in the ruptured aneurysms than the unruptured aneurysms. Among the unruptured cases, case D has a relative WSS closer to the ruptured cases

Further investigation with more aneurysm cases can help determine whether the additional flow separation indicated by LS is associated with aneurysm rupture.

Because flow simulation generates large amounts of data, and more importantly, because every aneurysm has its own unique shape, it is difficult to study descriptive hemodynamic results for a large patient study. In this paper we introduced a method using cut planes to extract data for the patient-specific CFD analysis. It takes approximately five minutes to perform the data analysis for each aneurysm. Moreover, by quantitatively documenting hemodynamic values, this method reduces subjective evaluations and increases efficiency for a larger study. Although certain local values may not be included because they are not covered by the cut plane, those local values usually continue

into the surrounding region and can still be captured by the nearest plane. More experiments using this approach will improve this method and its potential errors.

Wall shear stress, a frictional force acting parallel to the vessel wall, can elicit strong molecular biological responses [9, 14]. Recent reports suggested that WSS was associated with the initiation of brain aneurysms by inducing the focal degeneration of arterial walls [14, 17]. In the present study, we found that ruptured aneurysms tended to have a higher WSS distribution in the aneurysm sac than unruptured aneurysms. The physiological meaning of this finding remains unknown because the WSS was not absolutely high in the sac of ruptured aneurysms. The WSS in ruptured aneurysms was just relatively higher in the aneurysm sac than the WSS in unruptured aneurysm sacs (Fig. 5b). All of the aneurysms, ruptured or not, have WSS values in the parent arteries higher than in the aneurysm sac

($P < 0.001$). Further studies incorporating molecular responses to different levels of WSS may help clarify how relative WSS is related to aneurysm growth. Nevertheless, the present research suggests that the relative WSS value may be a useful hemodynamic parameter differing between ruptured and unruptured aneurysms.

In the quantitative analysis shown in Fig. 5b, results revealed that the ruptured aneurysms have significantly higher relative WSS at the aneurysm site ($P = 0.003$), averaging 72.3% (one is 74.4% and the other is 70.1%). The unruptured aneurysms have average relative WSS of 41.2% which includes one unruptured aneurysm with 63.6% relative WSS (case D). Currently, there is not sufficient information to explain whether case D is evidence of aneurysm growth in progress towards the rupture. Further analysis using a longitudinally followed database may help elucidate the role of relative WSS changes during aneurysm growth [24]. We believe the technique we presented is standardized enough to allow comparison of hemodynamics between aneurysms and can be applied to a larger clinical database to study the mechanism of brain aneurysm growth and rupture.

4.1 Limitations

In this study, we could only include six small aneurysms with a similar anatomical location after eliminating fusiform shaped aneurysms, large, and giant aneurysms. By choosing cases at a similar location with similar geometry, hemodynamic variation caused by other factors can be minimized; yet, we were able to find a trend of difference in hemodynamic parameters between ruptured and unruptured aneurysms. Our next task will be to combine patient data from other institutions and perform analysis with this methodology. In addition, since aneurysms at different locations may have different hemodynamic characteristics, current findings may only be applicable to small IC-Oph aneurysms. Similar hemodynamics studies for aneurysms at different locations also are needed.

Several assumptions have been made to help solve the flow equations, including the rigid boundary and the flow conditions. The rigid boundary assumption may result in higher shear stress values than with elastic boundaries, but general flow patterns should remain similar [1, 33]. Further research on the aneurysm wall tissue properties is important to incorporate the elastic boundary condition and yield a more accurate WSS calculation. The assumption of flow conditions scaled based on a normal subject may affect the value of flow velocity and WSS; however, the hemodynamic characteristics caused by geometry are still preserved [7]. In addition, because the flow conditions in the ophthalmic arteries are unknown, in the simulation a flow division based on the area was applied. It is possible

that the high WSS and high flow velocity observed in the ophthalmic arteries resulted from this outlet condition. Although previous studies have shown that the inclusion of small arteries in the model does not have a significant influence on hemodynamic characteristics [7], further identifying the flow conditions in the ophthalmic artery can help improve the IC-Oph models.

5 Conclusions

We perform hemodynamic analyses for aneurysms at a single location with similar size to reduce parameters which potentially influence the hemodynamic results. By using this method, we found that the relative value of WSS in an aneurysm sac may be an important hemodynamic parameter. We also showed that the presented approach can be useful to design a larger clinical study to investigate the role of hemodynamics in relationship with brain aneurysm growth and rupture.

References

1. Anayiotos AS, Jones SA, Giddens DP et al (1994) Shear stress at a compliant model of the human carotid bifurcation. J Biomech Eng 116:98–106. doi:10.1115/1.2895710
2. Beck J, Rohde S, el Beltagy M et al (2003) Difference in configuration of ruptured and unruptured intracranial aneurysms determined by biplanar digital subtraction angiography. Acta Neurochir (Wien) 145:861–865. doi:10.1007/s00701-003-0124-0 discussion 865
3. Burleson AC, Strother CM, Turitto VT (1995) Computer modeling of intracranial saccular and lateral aneurysms for the study of their hemodynamics. Neurosurgery 37:774–782. doi:10.1097/00006123-199510000-00023 discussion 782–774
4. Castro MA, Putman CM, Cebral JR (2006) Patient-specific computational modeling of cerebral aneurysms with multiple avenues of flow from 3D rotational angiography images. Acad Radiol 13:811–821. doi:10.1016/j.acra.2006.03.011
5. Cebral JR, Summers RM (2004) Tracheal and central bronchial aerodynamics using virtual bronchoscopy and computational fluid dynamics. IEEE Trans Med Imaging 23:1021–1033. doi:10.1109/TMI.2004.828680
6. Cebral JR, Castro MA, Burgess JE et al (2005) Characterization of cerebral aneurysms for assessing risk of rupture by using patient-specific computational hemodynamics models. AJNR Am J Neuroradiol 26:2550–2559
7. Cebral JR, Castro MA, Appanaboyina S et al (2005) Efficient pipeline for image-based patient-specific analysis of cerebral aneurysm hemodynamics: technique and sensitivity. IEEE Trans Med Imaging 24:457–467. doi:10.1109/TMI.2005.844159
8. Cebral JR, Castro MA, Putman CM et al (2008) Flow-area relationship in internal carotid and vertebral arteries. Physiol Meas 29:585–594. doi:10.1088/0967-3334/29/5/005
9. Cheng C, Tempel D, van Haperen R et al (2006) Atherosclerotic lesion size and vulnerability are determined by patterns of fluid shear stress. Circulation 113:2744–2753. doi:10.1161/CIRCULATIONAHA.105.590018

10. Jou LD, Quick CM, Young WL et al (2003) Computational approach to quantifying hemodynamic forces in giant cerebral aneurysms. AJNR Am J Neuroradiol 24:1804–1810

11. Kaazempur-Mofrad MR, Wada S, Myers JG et al (2005) Mass transport and fluid flow in stenotic arteries: Axisymmetric and asymmetric models. Int J Heat Mass Transfer 48:4510–4517. doi:10.1016/j.ijheatmasstransfer.2005.05.004

12. Murayama Y, Nien YL, Duckwiler G et al (2003) Guglielmi detachable coil embolization of cerebral aneurysms: 11 years' experience. J Neurosurg 98:959–966

13. Nomura M, Kida S, Uchiyama N et al (2000) Ruptured irregularly shaped aneurysms: pseudoaneurysm formation in a thrombus located at the rupture site. J Neurosurg 93:998–1002

14. Papaioannou TG, Karatzis EN, Vavuranakis M et al (2006) Assessment of vascular wall shear stress and implications for atherosclerotic disease. Int J Cardiol 113:12–18. doi:10.1016/j.ijcard.2006.03.035

15. Raghavan ML, Ma B, Harbaugh RE (2005) Quantified aneurysm shape and rupture risk. J Neurosurg 102:355–362

16. Reneman RS, Arts T, Hoeks AP (2006) Wall shear stress-an important determinant of endothelial cell function and structure-in the arterial system in vivo. Discrepancies with theory. J Vasc Res 43:251–269. doi:10.1159/000091648

17. Shojima M, Oshima M, Takagi K et al (2004) Magnitude and role of wall shear stress on cerebral aneurysm: computational fluid dynamic study of 20 middle cerebral artery aneurysms. Stroke 35:2500–2505. doi:10.1161/01.STR.0000144648.89172.0f

18. Shojima M, Oshima M, Takagi K et al (2005) Role of the bloodstream impacting force and the local pressure elevation in the rupture of cerebral aneurysms. Stroke 36:1933–1938. doi:10.1161/01.STR.0000177877.88925.06

19. Soto O, Löhner R, Cebral J et al (2004) A stabilized edge-based implicit incompressible flow formulation. Comput Methods Appl Mech Eng 193:2139–2154. doi:10.1016/j.cma.2004.01.018

20. Soustiel JF, Levy E, Bibi R et al (2001) Hemodynamic consequences of cerebral vasospasm on perforating arteries: a phantom model study. Stroke 32:629–635

21. Steinman DA, Milner JS, Norley CJ et al (2003) Image-based computational simulation of flow dynamics in a giant intracranial aneurysm. AJNR Am J Neuroradiol 24:559–566

22. Tateshima S, Murayama Y, Villablanca JP et al (2001) Intraaneurysmal flow dynamics study featuring an acrylic aneurysm model manufactured using a computerized tomography angiogram as a mold. J Neurosurg 95:1020–1027

23. Tateshima S, Murayama Y, Villablanca JP et al (2003) In vitro measurement of fluid-induced wall shear stress in unruptured cerebral aneurysms harboring blebs. Stroke 34:187–192. doi:10.1161/01.STR.0000046456.26587.8B

24. Tateshima S, Tanishita K, Omura H et al (2007) Intra-aneurysmal hemodynamics during the growth of an unruptured aneurysm: in vitro study using longitudinal CT angiogram database. AJNR Am J Neuroradiol 28:622–627

25. Tateshima S, Tanishita K, Omura H et al (2008) Intra-aneurysmal hemodynamics in a large middle cerebral artery aneurysm with wall atherosclerosis. Surg Neurol (in press). doi:10.1016/j.surneu.2008.03.035

26. The International Study of Unruptured Intracranial (1998) Unruptured intracranial aneurysms–risk of rupture and risks of surgical intervention. International Study of Unruptured Intracranial Aneurysms Investigators. N Engl J Med 339:1725–1733. doi:10.1056/NEJM199812103392401

27. Tobak M, Peake DJ (1982) Topology of three-dimensional separated flows. Ann Rev Fluid Mech 14:61–85. doi:10.1146/annurev.fl.14.010182.000425

28. Ujiie H, Tachibana H, Hiramatsu O et al (1999) Effects of size and shape (aspect ratio) on the hemodynamics of saccular aneurysms: a possible index for surgical treatment of intracranial aneurysms. Neurosurgery 45:119–129. doi:10.1097/00006123-199907000-00028 discussion 129–130

29. Ujiie H, Tamano Y, Sasaki K et al (2001) Is the aspect ratio a reliable index for predicting the rupture of a saccular aneurysm? Neurosurgery 48:495–502. doi:10.1097/00006123-200103000-00007 discussion 502–493

30. Wermer MJ, van der Schaaf IC, Algra A et al (2007) Risk of rupture of unruptured intracranial aneurysms in relation to patient and aneurysm characteristics: an updated meta-analysis. Stroke 38:1404–1410. doi:10.1161/01.STR.0000260955.51401.cd

31. Wiebers DO, Whisnant JP, Huston J 3rd et al (2003) Unruptured intracranial aneurysms: natural history, clinical outcome, and risks of surgical and endovascular treatment. Lancet 362:103–110. doi:10.1016/S0140-6736(03)13860-3

32. Yim P, Demarco K, Castro MA et al (2005) Characterization of shear stress on the wall of the carotid artery using magnetic resonance imaging and computational fluid dynamics. Stud Health Technol Inform 113:412–442

33. Zhao SZ, Xu XY, Hughes AD et al (2000) Blood flow and vessel mechanics in a physiologically realistic model of a human carotid arterial bifurcation. J Biomech 33:975–984. doi:10.1016/S0021-9290(00)00043-9